Computer Physics Communications 185 (2014) 1747–1758

Contents lists available at ScienceDirect

Computer Physics Communications

journal homepage: www.elsevier.com/locate/cpc

ShengBTE: A solver of the Boltzmann transport equation for phonons☆

Wu Li*, Jesús Carrete*,[1], Nebil A. Katcho, Natalio Mingo*,[2]

CEA, DRT, 38054 Grenoble, France

ARTICLE INFO

Article history:
Received 20 November 2013
Received in revised form
4 February 2014
Accepted 5 February 2014
Available online 26 February 2014

Keywords:
Boltzmann transport equation
Thermal conductivity
Phonon

ABSTRACT

ShengBTE is a software package for computing the lattice thermal conductivity of crystalline bulk materials and nanowires with diffusive boundary conditions. It is based on a full iterative solution to the Boltzmann transport equation. Its main inputs are sets of second- and third-order interatomic force constants, which can be calculated using third-party *ab-initio* packages. Dirac delta distributions arising from conservation of energy are approximated by Gaussian functions. A locally adaptive algorithm is used to determine each process-specific broadening parameter, which renders the method fully parameter free. The code is free software, written in Fortran and parallelized using MPI. A complementary Python script to help compute third-order interatomic force constants from a minimum number of *ab-initio* calculations, using a real-space finite-difference approach, is also publicly available for download. Here we discuss the design and implementation of both pieces of software and present results for three example systems: Si, InAs and lonsdaleite.

Program summary

Program title: ShengBTE
Catalogue identifier: AESL_v1_0
Program summary URL: http://cpc.cs.qub.ac.uk/summaries/AESL_v1_0.html
Program obtainable from: CPC Program Library, Queen's University, Belfast, N. Ireland
Licensing provisions: GNU General Public License, version 3
No. of lines in distributed program, including test data, etc.: 292 052
No. of bytes in distributed program, including test data, etc.: 1 989 781
Distribution format: tar.gz
Programming language: Fortran 90, MPI.
Computer: Non-specific.
Operating system: Unix/Linux.
Has the code been vectorized or parallelized?: Yes, parallelized using MPI.
RAM: Up to several GB
Classification: 7.9.
External routines: LAPACK, MPI, spglib (http://spglib.sourceforge.net/)
Nature of problem:
Calculation of thermal conductivity and related quantities, determination of scattering rates for allowed three-phonon processes

☆ This paper and its associated computer program are available via the Computer Physics Communication homepage on ScienceDirect (http://www.sciencedirect.com/science/journal/00104655).

* Corresponding authors.
E-mail addresses: wu.li.phys2011@gmail.com (W. Li), jcarrete@gmail.com (J. Carrete), natalio.mingo@cea.fr (N. Mingo).
[1] Tel.: +33 438780160.
[2] Tel.: +33 652837353.

http://dx.doi.org/10.1016/j.cpc.2014.02.015

Solution method:
Iterative solution, locally adaptive Gaussian broadening
Running time:
Up to several hours on several tens of processors

1. Introduction

The lattice thermal conductivity, denoted as κ_ℓ, is a key property in countless applications. Important technologies that demand specific materials with tailored thermal conductivities include thermoelectricity [1], heat management [2] and development of non-volatile memory based on phase-change materials [3]. Knowing how thermal conductivity changes under extreme conditions is also essential for understanding the behavior of the Earth's mantle [4]. Hence it is extremely desirable to have workflows available that yield predictive, parameter-free estimates of κ_ℓ using only basic information about the chemical structure of the crystal. Unfortunately, until recently the development of such approaches has been hindered both by methodological difficulties and by CPU time constraints, and to date no widely available software package exists to tackle this problem. Here we present a generic computer program to predict the lattice thermal conductivity of bulk crystalline materials and nanowires from first principles.

The main heat carriers in nonmagnetic crystals are phonons and electrons [5], with phonons dominating in semiconductors and insulators. The phonon-contributed part of the total thermal conductivity is the lattice thermal conductivity. Phonon properties including frequencies, velocities and scattering rates are largely determined by interatomic force constants (IFCs). One important approach to study phonon transport in solids is the Boltzmann transport equation (BTE) [5]. However, solving this equation is far from trivial. Although it was originally formulated by Peierls in 1929, even as late as in 1960 looking for a direct solution to the BTE was regarded as a hopeless endeavor [5]. Instead, many solutions to the BTE conventionally rely on the relaxation time approximation (RTA) along with the Debye approximation, neglecting the true phonon dispersions, and several parameters are introduced to treat different scattering mechanisms. To improve on this, Callaway proposed a model [6] that treats the quasimomentum-conserving normal processes and the non-quasimomentum-conserving Umklapp processes on a different footing. Very recently, an improvement upon Callaway's model has been proposed by Allen [7]. All these models involve parameters that are fitted to experimental data, and thus lack predictive power. In 1995 a practically feasible, iterative numerical method was proposed [8–10] to solve the BTE accurately. Early attempts started with a parameterized semiempirical interatomic potential, but such an approach suffers from problems of low accuracy and lack of transferability, since an appropriate potential for each compound must be developed.

In 2003, Deinzer et al. used density functional perturbation theory (DFPT) to perform a pioneering first-principles calculation of third-order IFCs in order to study the phonon linewidths of Si and Ge [11]. Later Broido et al. calculated κ_ℓ of these two elementary semiconductors by using *ab initio* IFCs and solving the BTE iteratively, achieving excellent agreement with experiments [12]. A systematic supercell approach for simultaneously obtaining the second- and third-order IFCs was introduced by Esfarjani and Stokes in 2008 [13]. In 2009, Tang and Dong used a supercell-based method to calculate anharmonic IFCs [14], and later they used those *ab-initio* IFCs to study the thermal conductivity of MgO within the RTA [15]. To date, *ab-initio* calculations of thermal conductivity have been applied to many bulk systems such as Si and Ge [12,16], diamond [17,18], MgO [15], Si_xGe_{1-x} [19], PbSe, PbTe, and $PbSe_xTe_{1-x}$ [20], Ga–V compounds [21], Mg_2Si, Mg_2Sn and $Mg_2Si_xSn_{1-x}$ [22], Al–V and In–V compounds [23], $MgSiO_3$ [24,25], and UO_2 [26]. All these applications show excellent agreement with experimental measurements. This combination of theoretical tools has recently been employed to predict that BAs has a thermal conductivity comparable to diamond [27]. Such calculations have also been applied to two-dimensional systems such as graphene [28] and MoS_2 [29]. An iterative solution for the BTE under diffusive boundary conditions has also been developed [30] and applied to nanowires made of Si, diamond [30], InAs, AlN and BeO [25]. Even though the RTA works well for some solids, an exact solution of BTE is generally necessary whenever normal three-phonon processes are relevant. The whole formalism for *ab-initio* thermal transport calculations is explained at length in Ref. [31].

In this paper we present a software package, `ShengBTE`,[3] able to solve the Boltzmann transport equation for phonons starting from a set of IFCs obtained *ab initio*. The program can compute converged sets of phonon scattering rates and use them to obtain κ_ℓ and many related quantities. `ShengBTE` harnesses the symmetries of the system to make these calculations more efficient and is able to deal with isotropic as well as anisotropic crystals. Moreover, it also implements an approximation developed by some of us to efficiently and accurately predict the thermal conductivity of nanowires under a diffusive boundary assumption [30].

Whereas computing harmonic IFCs is a standard functionality in many DFT packages, to the best of our knowledge there is no off-the-shelf software that can compute anharmonic IFCs. To complete our workflow, in addition to `ShengBTE` we also developed a script, `thirdorder.py`, implementing a real-space supercell approach to anharmonic IFC calculations. More specifically `thirdorder.py` can analyze the symmetries of the crystal and reduce the enormous number of DFT runs that would be required to characterize all relevant third-order derivatives of the energy to a mere few hundreds. The calculations themselves are delegated to a DFT package; currently that package is VASP [32] but adapting the code to the input and output formats of alternative DFT implementations such as Quantum Espresso [33] is straightforward. After these calculations have been run, reconstruction of the IFC set is fully automated. Both point-group and translational symmetries are enforced during this process. The latter is crucial for low-frequency behavior.

The latest releases of `ShengBTE` and `thirdorder.py` will be kept available at http://shengbte.org. Links to their Git repositories, hosting development versions and experimental features, can also be found there. Detailed compilation and usage instructions are included with both packages.

This paper is structured as follows. In Section 2 we introduce the mathematical formalism and methodological choices behind

[3] "Sheng" was chosen as part of the name of `ShengBTE` owing to its relation to the Chinese expressions for "phonon" and "sound". The sheng is also a Chinese wind instrument with a millenary history.

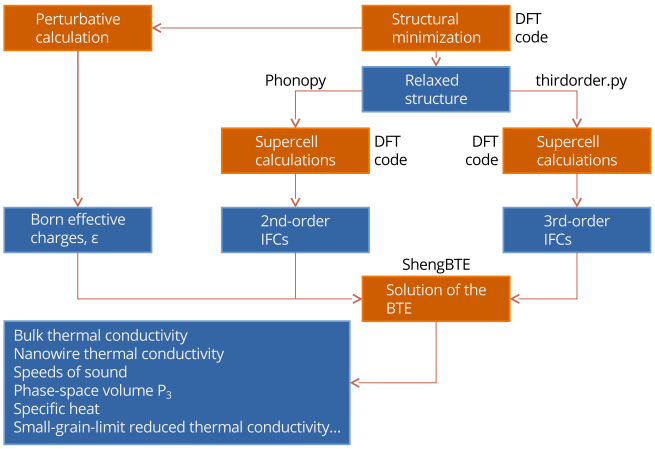

Fig. 1. Workflow for thermal conductivity calculations using a real-space supercell approach for force constants. Orange boxes represent steps of the calculations, blue boxes stand for the results of these steps, and computer programs are denoted as black text outside of any box. (For interpretation of the references to color in this figure legend, the reader is referred to the web version of this article.)

ShengBTE and `thirdorder.py`. Section 3 contains results for three different systems. Finally, we review our main conclusions in Section 4.

2. Methodology

2.1. *ShengBTE* workflow

The piece of software presented in this paper, along with the `thirdorder.py` script, enables completely *ab-initio* lattice thermal conductivity calculations. It is important to note, however, that such workflow can only be implemented in conjunction with other, preexisting programs. The two main inputs needed by ShengBTE are sets of second-order (harmonic) and third-order (anharmonic) force constants. As regards the former, our program relies completely on external tools to generate them and enforce the symmetries. Several approaches to harmonic IFC generation are implemented in publicly available software; they can be classified into the supercell and perturbative methods. ShengBTE accepts two different formats for second-order IFCs: that generated by Phonopy [34] (typically using a supercell and a variety of DFT back-ends) or the one created by Quantum Espresso [33] (most often employing DFPT). Harmonic constants coming from any other origin must be converted to either of these formats.

In contrast, we provide `thirdorder.py` to help compute third-order IFCs. It is based on a finite-difference supercell approach and it works in a manner similar to Phonopy: in the first step it generates a minimal set of displaced supercell configurations, then the user is expected to obtain forces for these configurations using DFT software, and finally the script gathers the results to rebuild the whole anharmonic IFC set.

An auxiliary element in the computation of the vibrational spectrum is a set of Born effective charges [35] together with an estimation of the dielectric tensor of the solid. With these two ingredients a long-range correction can be added to the dynamical matrix [36] in order to account for long-range electrostatic interactions in polar compounds. ShengBTE computes spectra matching those obtained by Phonopy or Quantum Espresso; hence, slightly different approximations are used depending on the source of harmonic IFCs. For force constants coming from Quantum Espresso we implement the scheme by Gonze et al. [37], based on an Ewald summation; when force constants have been generated with Phonopy we use the method proposed by Wang et al. [38]. The latter has been devised specifically to work with supercell-based, finite-difference approaches to second-order IFC calculations. It takes into account that frequencies calculated at points of reciprocal space that are commensurate with the supercell are exact, so any long-range correction must vanish at those points. Both methods recover the known analytical limit of the long-range correction at Γ and serve as approximate interpolation schemes for general points in the Brillouin zone. Both have been shown to yield good agreement with experiment [37,38]. Hence, as long as the quality of the force constants and dielectric parameters used as inputs is similar, ShengBTE's results should be comparable regardless of which method is employed. This assertion has been tested directly for a few representative cases.

For the examples presented in this paper we used Phonopy to obtain second-order IFCs and VASP for all DFT calculations. Born effective charges were also computed using the perturbative approach implemented in VASP. A summary of our workflow, starting with the determination of the relaxed structure of each solid and ending with the calculation of κ_ℓ, is sketched in Fig. 1. The following subsections are related to the parts of this workflow implemented in our software.

2.2. The BTE

A non-zero heat current $\mathbf{J}$ can arise from a temperature gradient ∇T. In the linear regime, the components of $\boldsymbol{\kappa}$ are defined by the equation $J^\alpha = -\sum_\beta \kappa^{\alpha\beta} (\nabla T)^\beta$. $\mathbf{J}$ can be obtained as

$$\mathbf{J} = \sum_p \int f_\lambda \hbar \omega_\lambda \mathbf{v}_\lambda \frac{d\mathbf{q}}{(2\pi)^3} \tag{1}$$

where λ comprises both a phonon branch index p and a wave vector $\mathbf{q}$, ω_λ and $\mathbf{v}_\lambda$ are the angular frequency and group velocity of phonon mode λ, respectively, and f_λ is the phonon distribution function. At thermal equilibrium, in the absence of a temperature gradient or other thermodynamical forces, phonons are distributed according to Bose–Einstein statistics $f_0(\omega_\lambda)$. In the presence of a temperature gradient ∇T, f deviates from f_0, and this deviation can be obtained from the BTE. Two factors affect the phonon distribution: diffusion due to ∇T and scattering arising from allowed processes. In the steady state, the rate of change in the distribution must vanish; this condition is expressed by the BTE [39,5]:

$$\frac{df_\lambda}{dt} = \left.\frac{\partial f_\lambda}{\partial t}\right|_{\text{diffusion}} + \left.\frac{\partial f_\lambda}{\partial t}\right|_{\text{scattering}} = 0, \tag{2}$$

where

$$\left.\frac{\partial f_\lambda}{\partial t}\right|_{\text{diffusion}} = -\nabla T \cdot \mathbf{v}_\lambda \frac{\partial f_\lambda}{\partial T}, \tag{3}$$

and $\partial f_\lambda/\partial t|_{\text{scattering}}$ depends on the specific scattering processes, which can be analyzed in the framework of perturbation theory. In single crystals, phonons are scattered mainly due to phonon–phonon interactions and impurities such as isotopes [5]. Due to the finite character of real bulk samples, at very low temperatures boundary scattering can play a significant role. Nevertheless, its treatment is not included in the present discussion.

In most practical situations, the norm of ∇T is small enough that f_λ can be expanded to first order in ∇T so that $f_\lambda = f_0(\omega_\lambda) + g_\lambda$, where g_λ depends on ∇T linearly. We can choose to express this dependence as $g_\lambda = -\mathbf{F}_\lambda \cdot \nabla T \frac{df_0}{dT}$. When the only scattering sources are the two- and three-phonon processes, the resulting linearized BTE can then be written as [8,9,40,17,16]:

$$\mathbf{F}_\lambda = \tau_\lambda^0 (\mathbf{v}_\lambda + \boldsymbol{\Delta}_\lambda). \tag{4}$$

Here, τ_λ^0 is the relaxation time of mode λ as obtained from perturbation theory and commonly used within the RTA. In fact, as will be explained in detail in what follows, setting all $\boldsymbol{\Delta}_\lambda$ to zero in Eq. (4) is equivalent to working within the RTA. Hence $\boldsymbol{\Delta}_\lambda$, with the dimensions of velocity, is the measure of how much the population of a specific phonon mode – and thus the associated heat current – deviates from the RTA prediction. More explicitly, $\boldsymbol{\Delta}_\lambda$ and τ_λ^0 are computed as

$$\begin{aligned}\boldsymbol{\Delta}_\lambda = & \frac{1}{N}\sum_{\lambda'\lambda''}^{+}\Gamma^{+}_{\lambda\lambda'\lambda''}\left(\xi_{\lambda\lambda''}\mathbf{F}_{\lambda''}-\xi_{\lambda\lambda'}\mathbf{F}_{\lambda'}\right)\\ & +\frac{1}{N}\sum_{\lambda'\lambda''}^{-}\frac{1}{2}\Gamma^{-}_{\lambda\lambda'\lambda''}\left(\xi_{\lambda\lambda''}\mathbf{F}_{\lambda''}+\xi_{\lambda\lambda'}\mathbf{F}_{\lambda'}\right)\\ & +\frac{1}{N}\sum_{\lambda'}\Gamma_{\lambda\lambda'}\xi_{\lambda\lambda'}\mathbf{F}_{\lambda'},\end{aligned} \tag{5}$$

$$\frac{1}{\tau_\lambda^0}=\frac{1}{N}\left(\sum_{\lambda'\lambda''}^{+}\Gamma^{+}_{\lambda\lambda'\lambda''}+\sum_{\lambda'\lambda''}^{-}\frac{1}{2}\Gamma^{-}_{\lambda\lambda'\lambda''}+\sum_{\lambda'}\Gamma_{\lambda\lambda'}\right), \tag{6}$$

where we introduce a discretization of the Brillouin zone (BZ) into a Γ-centered regular grid of $N = N_1 \times N_2 \times N_3$ $\mathbf{q}$ points, and use the shorthand $\xi_{\lambda\lambda'} = \omega_{\lambda'}/\omega_\lambda$. Conservation of quasimomentum requires that $\mathbf{q}'' = \mathbf{q} \pm \mathbf{q}' + \mathbf{Q}$ in the summation $\sum^{\pm}$ for some reciprocal-lattice vector $\mathbf{Q}$ such that $\mathbf{q}''$ is in the same image of the Brillouin zone as $\mathbf{q}$ and $\mathbf{q}'$. The regularity of the sampling grid guarantees that it also contains $\mathbf{q}''$. The notation employed here differs slightly from the one used in previous publications from some of the authors [41,22] in which the group velocity was not included in $\boldsymbol{\Delta}_\lambda$.

The quantities $\Gamma^{\pm}_{\lambda\lambda'\lambda''}$ in Eq. (6) are three-phonon scattering rates, and can be expressed as

$$\Gamma^{+}_{\lambda\lambda'\lambda''}=\frac{\hbar\pi}{4}\frac{f_0'-f_0''}{\omega_\lambda\omega_{\lambda'}\omega_{\lambda''}}\left|V^{+}_{\lambda\lambda'\lambda''}\right|^2\delta\left(\omega_\lambda+\omega_{\lambda'}-\omega_{\lambda''}\right) \tag{7}$$

$$\Gamma^{-}_{\lambda\lambda'\lambda''}=\frac{\hbar\pi}{4}\frac{f_0'+f_0''+1}{\omega_\lambda\omega_{\lambda'}\omega_{\lambda''}}\left|V^{-}_{\lambda\lambda'\lambda''}\right|^2\delta\left(\omega_\lambda-\omega_{\lambda'}-\omega_{\lambda''}\right), \tag{8}$$

where, for simplicity, f_0' stands for $f_0(\omega_{\lambda'})$ and so forth. $\Gamma^{+}_{\lambda\lambda'\lambda''}$ corresponds to absorption processes, resulting in only one phonon with the combined energy of two incident phonons ($\omega_\lambda + \omega_{\lambda'} = \omega_{\lambda''}$) whereas $\Gamma^{-}_{\lambda\lambda'\lambda''}$ describes emission processes in which the energy of one incident phonon is split among two phonons ($\omega_\lambda = \omega_{\lambda'} + \omega_{\lambda''}$). Conservation of energy in the absorption and emission processes is enforced by the Dirac delta distributions in Eqs. (7) and (8). To successfully compute the values of $\Gamma^{\pm}_{\lambda\lambda'\lambda''}$ we need the scattering matrix elements $V^{\pm}_{\lambda\lambda'\lambda''}$, given by [40,17]

$$V^{\pm}_{\lambda\lambda'\lambda''}=\sum_{i\in\text{u.c.}}\sum_{j,k}\sum_{\alpha\beta\gamma}\Phi^{\alpha\beta\gamma}_{ijk}\frac{e^{\alpha}_{\lambda}(i)\,e^{\beta}_{p',\pm\mathbf{q}'}(j)\,e^{\gamma}_{p'',-\mathbf{q}''}(k)}{\sqrt{M_iM_jM_k}}; \tag{9}$$

these in turn depend on the normalized eigenfunctions $\mathbf{e}_{p,\mathbf{q}}$ of the three phonons involved and on the anharmonic IFCs $\Phi^{\alpha\beta\gamma}_{ijk}=\frac{\partial^3 E}{\partial r_i^\alpha \partial r_j^\beta \partial r_k^\gamma}$. In these expressions, i, j and k run over atomic indices while α, β and γ denote Cartesian coordinates. In the sums, i only runs over the atoms in what we shall call the central unit cell, but j and k cover the whole system. r_i^α and M_i denote the α component of the displacement from the equilibrium position and the mass of the ith atom, respectively. Finally, $e^{\alpha}_{\lambda}(i)$ is the α component of the eigenfunction of mode λ at the ith atom.

Apart from three-phonon processes, we also include the contribution to scattering probabilities from isotopic disorder, with rates given by [42,41]:

$$\Gamma_{\lambda\lambda'}=\frac{\pi\omega^2}{2}\sum_{i\in\text{u.c.}}g(i)\left|\mathbf{e}^{*}_{\lambda}(i)\cdot\mathbf{e}_{\lambda'}(i)\right|^2\delta\left(\omega_\lambda-\omega_{\lambda'}\right), \tag{10}$$

where $g(i)=\sum_s f_s(i)\left[1-M_s(i)/\overline{M}(i)\right]^2$ is the Pearson deviation coefficient of the masses $M_s(i)$ of isotopes s of atom i (found with relative frequency $0 < f_s(i) \leq 1$) and $\overline{M}(i)=\sum_s f_s(i)M_s(i)$ their average. For instance, the natural isotopic distributions [43] of Si yield a value of $g(i)$ of 2.007×10^{-4}.

κ_ℓ can be obtained in terms of $\mathbf{F}$ as

$$\kappa_\ell^{\alpha\beta}=\frac{1}{k_B T^2 \Omega N}\sum_{\lambda}f_0\left(f_0+1\right)(\hbar\omega_\lambda)^2 v_\lambda^\alpha F_\lambda^\beta, \tag{11}$$

where Ω is the volume of the unit cell. In the approach implemented in ShengBTE, Eq. (4) is solved iteratively starting with a zeroth-order approximation $\mathbf{F}_\lambda^0 = \tau_\lambda^0\mathbf{v}_\lambda$. The stopping criterion is that the relative change in the conductivity tensor calculated using Eq. (11), as measured using the Frobenius norm, is less than a configurable parameter with a default value of 10^{-5}. Stopping at the zeroth iteration is tantamount to operating under the RTA. The iterative process can have a large impact on the results when studying high-κ_ℓ materials like diamond where normal three-phonon processes play an important role, as the RTA deals with normal processes as resistive [17]. However, in systems like Si and Ge, with strong Umklapp scattering, iterating to convergence typically adds less than 10% to the room-temperature thermal conductivity when compared to the RTA result [16].

Calculation of $\Gamma^{\pm}_{\lambda\lambda'\lambda''}$ can take a great amount of time. However, by harnessing symmetry, only those $\mathbf{q}$ points lying inside the irreducible wedge of the BZ need to be selected from the full grid. In order to maximize the effect of such reduction N_1, N_2 and N_3 must be chosen in such a way that the space group symmetry of the crystal structure under consideration is preserved; a particular choice guaranteeing this is $N_1 = N_2 = N_3$. Automatic symmetry detection is implemented in ShengBTE by calling functions in Atsushi Togo's `spglib` [44].

2.3. Nanowires

Crystalline nanowires are only periodic along one direction, and strictly speaking their phonon dispersions must be expressed as functions of the wave number along that direction alone. However, for nanowires thick enough to comprise a significant number of unit cells in the transverse directions the number of phonon branches is very high and the bulk phonon dispersions can be used instead. This does not change the fact that physical boundaries break the translational symmetry perpendicular to the nanowire axis, so phonon lifetimes are position-dependent and the BTE has an additional space-dependent term. Eq. (4) must be generalized to

$$\mathbf{F}_{\mathbf{r},\lambda}=\tau_\lambda^0\left\{\boldsymbol{\Delta}_{\mathbf{r},\lambda}+\mathbf{v}_\lambda\left[1-\frac{1}{|\mathbf{v}_\lambda|^2}\left(\mathbf{v}_\lambda\cdot\nabla\right)\left(\mathbf{v}_\lambda\cdot\mathbf{F}_{\mathbf{r},\lambda}\right)\right]\right\}, \tag{12}$$

where the dependence of $\boldsymbol{\Delta}_{\mathbf{r},\lambda}$ on $\mathbf{F}_{\mathbf{r},\lambda}$ is the same as that of $\boldsymbol{\Delta}_\lambda$ on $\mathbf{F}_\lambda$, expressed in Eq. (5). The computational cost of solving Eq. (12) as a space-dependent equation is disproportionately high compared to Eq. (4). To tackle this problem, some of us developed an approximate iterative solution to Eq. (12) that is discussed in detail elsewhere [30]. The philosophy of this approach is to focus on the long direction of the nanowire and use cross-sectional averages to partially remove the remaining two spatial degrees of freedom from the treatment.

Since we are only interested in thermal transport along the unbounded direction of the nanowire, we can simplify the notation by treating $F_{\mathbf{r},\lambda}$, v_λ and $\Delta_{\mathbf{r},\lambda}$ as scalars. The approximate solution to Eq. (12) implemented in ShengBTE starts by replacing $\Delta_{\mathbf{r},\lambda}$ by

its average value over the cross section ($\overline{\Delta}_\lambda$) leading to the formal solution to the BTE developed by Chambers [45]:

$$F_{\mathbf{r},\lambda} = \tau^0_\lambda \left(v_\lambda + \overline{\Delta}_\lambda\right) \left\{1 - e^{-\left|\frac{\mathbf{r}-\mathbf{r}_b}{\tau^0 v_\lambda}\right|} G_{\mathbf{r},\lambda}\right\}, \tag{13}$$

where $\mathbf{r}_b$ is the point on the surface of the nanowire that a phonon in mode λ can reach by moving backwards from $\mathbf{r}$, and $G_{\mathbf{r},\lambda}$ is determined by the boundary conditions. For completely diffusive boundary scattering, as considered here, $G_{\mathbf{r},\lambda} = 1$. The average of $F_{\mathbf{r},\lambda}$ over the cross section, $\overline{F}_\lambda$, can thus be obtained as

$$\overline{F}_\lambda = \tau^0_\lambda \left(v_\lambda + \overline{\Delta}_\lambda\right) \frac{1}{S_c} \int_{S_c} \left\{1 - e^{-\left|\frac{\mathbf{r}-\mathbf{r}_b}{\tau^0 v_\lambda}\right|}\right\} d\mathbf{s}, \tag{14}$$

by integration over the cross-section of the nanowire, S_c. Again, this can be solved iteratively starting from the RTA solution

$$\overline{F}^0_\lambda = \frac{F^0_\lambda}{S_c} \int_{S_c} \left\{1 - e^{-\left|\frac{\mathbf{r}-\mathbf{r}_b}{\tau^0 v_\lambda}\right|}\right\} d\mathbf{s}. \tag{15}$$

Finally, replacing F_λ with $\overline{F}_\lambda$ in Eq. (11) yields the nanowire thermal conductivity.

2.4. Conservation of energy

Most three-phonon scattering processes fulfilling one of the conditions $\omega_\lambda - (\pm\omega_{\lambda'} + \omega_{\lambda''}) = 0$, for a given ω_λ, involve modes λ' and λ'' that are not sampled by the $N_1 \times N_2 \times N_3$ $\mathbf{q}$-point grid. Hence, Eqs. (7) and (8) cannot be directly inserted into the sums over the regular grid required by Eqs. (5) and (6), because the Dirac deltas that they contain are identically zero with high probability for every triplet $(\lambda, \lambda', \lambda'')$ sampled.

A possible solution is to abandon the idea of getting the second and third phonons involved in the process from the same regular grid, and instead interpolate the dispersion relations in order to solve $\omega_\lambda - (\pm\omega_{\lambda'} + \omega_{\lambda''}) = 0$ and look for allowed processes. This approach has been successfully employed in Refs. [40,17,16,23,21,27]. While this approach is potentially very accurate, it is also computationally very demanding. An appealing alternative is to regularize the Dirac delta by substituting it by a finite-breadth approximation, of which one of the most common is a Gaussian function

$$g\left(\omega_\lambda - W\right) = \frac{1}{\sqrt{2\pi}\sigma} e^{-\frac{(\omega_\lambda - W)^2}{2\sigma^2}}. \tag{16}$$

Naturally, it would be desirable to use a σ as small as possible so as to approach the ideal Dirac delta; however, it cannot be too small or the probability of not having enough phonon scattering channels would be high. Leaving σ as an adjustable parameter is not acceptable as it would allow one to tune the result arbitrarily and defeat the purpose of having a parameter-free approach. It is desirable to implement an algorithm that will automatically use the right value of σ under general circumstances.

Integrals over $\mathbf{q}'$ of functions depending on $\Gamma_{\lambda\lambda'\lambda''}$ are smooth functions of $\mathbf{q}$. In order to avoid not only any spurious strong oscillation due to the approximation of an integral by a sum such as those in Eqs. (5) and (6), but also any oversmoothing of the Delta distributions leading to the inclusion of unphysical scattering processes, the spread of each Gaussian as measured by σ has to be chosen so as to approximate the standard deviation of W in the region of reciprocal space around each $\mathbf{q}'$ point resulting from the actual phonon dispersions for a given λ [30]. Since $\mathbf{q}'$ and $\mathbf{q}''$ are bound by conservation of quasimomentum, W can be written as a function of just one of them, for instance as $W\left(\mathbf{q}'\right)$. Its mean and variance can be extracted from a first-order Taylor expansion around a mesh point $\mathbf{q}'_0$:

$$\begin{aligned} W &\simeq W\left(\mathbf{q}'_0\right) + \sum_\mu \frac{\partial W}{\partial \mathrm{q}'^\mu} \left(\mathrm{q}'^\mu - \mathrm{q}'^\mu_0\right) \\ \overline{W} &= E\{W\} \simeq W\left(\mathbf{q}'_0\right) \\ \sigma^2_W &= E\left\{\left(W - \overline{W}\right)^2\right\} \simeq E\left\{\left[W - W\left(\mathbf{q}'_0\right)\right]^2\right\} \\ &\simeq \sum_\mu \left(\frac{\partial W}{\partial \mathrm{q}'^\mu}\right)^2 E\left\{\left(\mathrm{q}'^\mu - \mathrm{q}'^\mu_0\right)^2\right\}. \end{aligned} \tag{17}$$

Here, q'^μ is the projection of $\mathbf{q}'$ over reciprocal-space lattice vector $\mathbf{Q}_\mu$, whose component along Cartesian axis α we will denote as Q^α_μ in what follows, and $E\{x\}$ denotes the mathematical expectation of x. The mathematical expectation in the last term is the variance of each component of $\mathbf{q}'$ in a mesh cell, whose square root is equal to the side of the cell in that direction over a factor $\sqrt{12}$. This yields

$$\begin{aligned} \sigma_W &\simeq \sqrt{\sum_\mu \left(\frac{\partial W}{\partial \mathrm{q}'^\mu} \frac{\Delta \mathrm{q}'^\mu}{\sqrt{12}}\right)^2} \\ &= \frac{1}{\sqrt{12}} \sqrt{\sum_\mu \left[\sum_\alpha \left(v^\alpha_{\lambda'} - v^\alpha_{\lambda''}\right) \frac{Q^\alpha_\mu}{N_\mu}\right]^2}. \end{aligned} \tag{18}$$

In ShengBTE we use this estimate of σ_W times a proportionality constant `scalebroad` as the σ for each point. That constant defaults to unity as a safe choice, but often convergence can be achieved using significantly smaller values, with notable gains in speed. The correlation between `scalebroad` and speed of execution stems from the fact that the amplitude of each Gaussian is approximated by zero, as an optimization, for any point situated at more than 2σ from its mean. Thus, the lower `scalebroad` is the fewer three-phonon scattering processes that need to be considered. A similar broadening scheme is employed for the Dirac delta distribution arising from isotope scattering, as described in Eq. (10). Naturally, convergence with the number of $\mathbf{q}$ points still needs to be checked.

2.5. Other integrals

Although κ_ℓ for the bulk and for nanowires can be considered to be the main result from ShengBTE, a number of related physical quantities and theoretical descriptors are also computed to give the user additional insight. The simplest one is the specific heat per unit volume in the harmonic approximation,

$$\begin{aligned} c_v &= \frac{k_B}{\Omega N} \sum_\lambda \left(\frac{\hbar\omega}{k_B T}\right)^2 f_0\left(f_0 + 1\right) \\ &= \frac{k_B}{(2\pi)^3} \int_{BZ} \left(\frac{\hbar\omega}{k_B T}\right)^2 f_0\left(f_0 + 1\right) d^3\mathbf{q}. \end{aligned} \tag{19}$$

Another integral related to κ_ℓ that, like c_v, depends only on harmonic properties, is the small-grain-limit reduced thermal conductivity, $\tilde{\kappa}_{SG}$. When nanostructuring is introduced in a bulk material, a new contribution to phonon scattering rates appears, associated to a mean free path of the order of magnitude of the nanostructure size. As this size is made smaller this can become the dominant contribution, so the mean free path is uniformly limited to a constant value Λ. This amounts to substituting $F^\beta_\lambda = \Lambda v^\beta_\lambda / |\mathbf{v}_\lambda|$ into Eq. (11), after which κ_ℓ becomes proportional to Λ; $\tilde{\kappa}_{SG}$ is defined as the proportionality tensor

$$\tilde{\kappa}^{\alpha\beta}_{SG} = \frac{1}{k_B T^2 \Omega N} \sum_\lambda f_0\left(f_0 + 1\right) \frac{v^\alpha_\lambda v^\beta_\lambda}{|\mathbf{v}_\lambda|} \hbar^2 \omega^2_\lambda. \tag{20}$$

This quantity can give an idea of the influence of the harmonic properties of the solid on its conductivity. It is also strongly correlated with the conductivity of nanostructures, for example nanowires.

More generally, it is often useful to be able to determine the mean free path of those phonons that are most relevant to thermal conduction. For this, ShengBTE also outputs the cumulative thermal conductivity, *i.e.*, the value of κ_ℓ when only phonons with mean free paths below a threshold are considered. Our definition of the scalar mean free path for mode λ is

$$\Lambda_\lambda = \frac{\mathbf{F}_\lambda \cdot \mathbf{v}_\lambda}{|\mathbf{v}_\lambda|}. \tag{21}$$

To understand this definition, note that if we replace $\mathbf{F}_\lambda$ in Eq. (11) by $\mathbf{v}_\lambda \tau_\lambda^0$, whose modulus is the usual RTA definition of the mean free path (Λ_λ^0) we obtain the RTA expression of the thermal conductivity. Thus, $\mathbf{F}_\lambda$ plays the role of a vectorial "mean free displacement", but in contrast with $\mathbf{v}_\lambda \tau_\lambda^0$ it does not have to be parallel to the group velocity of the mode. Our definition of a scalar mean free path follows logically from this idea, as the projection of this "mean free displacement" along the direction of energy transport. As opposed to Λ_λ^0, this Λ_λ can be positive or negative. This is a consequence of the fact that the deviation from equilibrium of the phonon distribution for a mode (g_λ) can have both signs in the full BTE framework considered here, but always has the same one in the RTA. For the same reason, one cannot define a positive relaxation time that captures all the information about scattering, and full knowledge of $\mathbf{F}_\lambda$ is required instead. Nevertheless, for low frequencies the mean free path defined in Eq. (21) will always be positive. On physical grounds this is to be expected from those modes that contribute the most to thermal transport. It can also be derived more formally from Eq. (4): when the norm of the group velocity of a mode is high, the perturbation introduced by $\boldsymbol{\Delta}_\lambda$ is not enough to cause the projection of $\mathbf{F}_\lambda$ over its RTA value to be negative. More generally, in situations where the RTA is a reasonable approximation modes with negative values of the mean free path will be few, if any.

Part of what makes the lattice thermal conductivity of a material high or low is the fraction of three-phonon processes that are allowed by conservation of energy. This factor, sometimes called the "phase space" [40], can be analyzed in isolation by removing the probabilities of individual processes from the picture. The result is the integral

$$P_3 = \frac{\Omega}{(6\pi n)^3} \sum_{p,p',p''} \iint_{BZ} \delta\left[\omega_p(\mathbf{q}) + \omega_{p'}(\mathbf{q}') - \omega_{p''}(\mathbf{q}+\mathbf{q}'-\mathbf{Q})\right] d^3\mathbf{q}' d^3\mathbf{q}. \tag{22}$$

It is easy to check that $0 \le P_3 \le 1$; actual values are several orders of magnitude lower than the upper bound and are known to have a strong negative correlation [40] with κ_ℓ. Our program outputs the global value of P_3 as well as the contributions from each mode and each $\mathbf{q}$ point in the grid.

Finally, ShengBTE also obtains the phonon density of states (DOS) and its projection over each atom in the system (PDOS) using the same adaptive smearing scheme presented above.

2.6. Third-order IFCs

For small displacements, the total potential energy of the system can be expanded into

$$E = E_0 + \frac{1}{2}\sum_{\substack{ij\\ \alpha\beta}} \Phi_{ij}^{\alpha\beta} r_i^\alpha r_j^\beta + \frac{1}{3!}\sum_{\substack{ijk\\ \alpha\beta\gamma}} \Phi_{ijk}^{\alpha\beta\gamma} r_i^\alpha r_j^\beta r_k^\gamma. \tag{23}$$

The coefficients Φ in the n-th order term are the corresponding n-th order IFCs. As for the third-order IFCs, translational symmetry means that IFCs do not depend directly on the absolute coordinates of atom triplet (i, j, k), but only on the relative coordinates of the three atoms. Thus, we only need to consider the elements for which i is limited to one unit cell for convenience.

In `thirdorder.py` we use a supercell-based, finite-difference method to calculate the third-order IFCs:

$$\begin{aligned}\Phi_{ijk}^{\alpha\beta\gamma} &= \frac{\partial^3 E}{\partial r_i^\alpha \partial r_j^\beta \partial r_k^\gamma} \\ &\simeq \frac{1}{2h}\left[\frac{\partial^2 E}{\partial r_j^\beta \partial r_k^\gamma}(r_i^\alpha = h) - \frac{\partial^2 E}{\partial r_j^\beta \partial r_k^\gamma}(r_i^\alpha = -h)\right] \\ &\simeq \frac{1}{4h^2}\Big[-F_k^\gamma(r_i^\alpha = h, r_j^\beta = h) + F_k^\gamma(r_i^\alpha = h, r_j^\beta = -h) \\ &\quad + F_k^\gamma(r_i^\alpha = -h, r_j^\beta = h) - F_k^\gamma(r_i^\alpha = -h, r_j^\beta = -h)\Big],\end{aligned} \tag{24}$$

where h is a small displacement from the equilibrium position, and F_k^γ is the γ component of the force felt by the k-th atom. The default value of h is 0.04 times the Bohr radius, or $2.12 \cdot 10^{-3}$ nm, but it can be easily changed by editing the header of the `thirdorder.py` script. Each element of $\Phi_{ijk}^{\alpha\beta\gamma}$ requires four DFT calculations with different supercell configurations, and there are $27n^3\mathcal{N}^2$ anharmonic IFCs for a unit cell with n atoms and a supercell with $\mathcal{N}$ unit cells. Considering that all the forces experienced by all atoms in the supercell can be obtained in a single DFT run, naively $4 \times 9n^2\mathcal{N}$ DFT runs would be required. A typical calculation demands supercells easily exceeding ~100 atoms, meaning that several thousand DFT runs would be needed. This is impractical for most computing infrastructures. However, the number of IFCs that need to be calculated can be significantly reduced if we take advantage of symmetries.

When speaking of symmetries, we include both point-group symmetries and the invariance ("permutation symmetry") of $\Phi_{ijk}^{\alpha\beta\gamma}$ under any permutation of pairs (i, α), (j, β) and (k, γ) arising from the equality of mixed partials. Let us consider a general space-group symmetry operation $\sum_\alpha T^{\alpha'\alpha} R_i^\alpha + b^{\alpha'} = R_{Tb(i)}^{\alpha'}$, where $\mathbf{T}$ and $\mathbf{b}$ stand for the point-group and translation operators respectively, and $T_{b(i)}$ specifies the atom to which the ith atom is mapped under the corresponding operation. The third-order IFC tensor must satisfy the following relation:

$$\Phi_{T_{b(i)};T_{b(j)};T_{b(k)}}^{\alpha'\beta'\gamma'} = \sum_{\alpha\beta\gamma} T^{\alpha'\alpha} T^{\beta'\beta} T^{\gamma'\gamma} \Phi_{ijk}^{\alpha\beta\gamma}. \tag{25}$$

Each symmetry operation, including the permutation and space-group symmetries, can either map the three atom indices $\{i, j, k\}$ into themselves or to a different set. The first class of operations imposes m constraints on the set of 27 anharmonic IFCs associated to an atomic triplet. Using Gaussian elimination, the m linear equations describing these constraints can be transformed into a form like

$$\begin{pmatrix} 1 & 0 & * & 0 & 0 & \dots \\ 0 & 1 & * & 0 & 0 & \dots \\ 0 & 0 & 0 & 1 & 0 & \dots \\ 0 & 0 & 0 & 0 & 1 & \dots \\ \vdots & \vdots & \vdots & \vdots & \vdots & \vdots \end{pmatrix} \begin{pmatrix} x_1 \\ x_2 \\ \vdots \\ x_{27} \end{pmatrix} = 0, \tag{26}$$

where the columns with asterisks (which stand for arbitrary numbers) correspond to the independent elements among the set of 27 IFCs. The remaining force constants can be reconstructed as linear combinations of them. In practice, a cutoff radius is defined such that atoms further away than the cutoff are considered noninteracting.

In summary, reducing the number of anharmonic IFCs to be calculated involves three steps. The first one consists in choosing a cutoff radius, which limits the number of triplets to be considered. Second, triplets are grouped into equivalence classes by means of symmetries. Finally, a representative triplet is chosen from each class and the number of independent IFCs associated to it is further reduced (from the original 27), again by making use of symmetries. Like ShengBTE, `thirdorder.py` relies on the `spglib` library for detecting crystal symmetries.

Generally speaking, convergence with respect to the cutoff radius has to be checked manually, either by looking at the force constants directly or by inspection of the calculated thermal conductivities. For many zinc-blende crystals we have found that including up to third nearest neighbors gives a satisfactorily converged value of κ_ℓ.

It must be borne in mind that anharmonic IFCs are derivatives of harmonic IFCs, so a consistent calculation requires that both sets of IFCs are obtained using similar parameters (approximations to exchange and correlation, pseudopotentials, lattice parameters, parameterization of the unit cell and so on). As an example, using the local density approximation (LDA) for the second-order IFCs and the generalized gradient approximation (GGA) for the third-order ones will result in an overestimation of the thermal conductivity for most systems. This is because of the well known tendency of LDA to underestimate bond lengths and overestimate bonding energies, whereas the opposite is true for GGA. Since the harmonic and anharmonic IFCs are derivatives of the energy, as a general rule both sets of constants will be larger in magnitude when computed using the LDA [46,21,47,48]. In other words, the LDA will tend to overestimate phonon frequencies and scattering rates, whereas the GGA will generally underestimate both.

2.7. Sum rules for the anharmonic IFCs

Invariance of Eq. (23) with respect to any global displacement requires that

$$\sum_k \Phi_{ijk}^{\alpha\beta\gamma} = 0. \tag{27}$$

Due to permutation symmetries, this is also valid if the summation is performed over i or j.

The fact that these sums are exactly zero is crucial to obtaining the right scattering rates at low frequencies. Generally the force constants computed by *ab-initio* packages do not satisfy these sum rules exactly, especially when a cutoff radius is introduced, and thus some kind of manipulation is needed to enforce them while at the same time changing the IFCs only slightly. The general idea is to add a small compensation to each independent non-zero IFC so that these conditions are satisfied. A reasonable (even if not univocal) choice is to minimize the sum of squares of these compensations [22], which results in a well-posed constrained minimization problem.

Nevertheless, it is not necessary to enforce all sum rules *a posteriori*: some of them will be satisfied automatically by the partially symmetrized anharmonic IFCs. Even the non-zero sums remaining are not all fully independent, but a minimal set of independent equations can easily be found numerically. If – to avoid excessive notation – we summarize in a single index J the three superscripts and the three subscripts $\begin{pmatrix}\alpha & \beta & \gamma\\ i & j & k\end{pmatrix}$ required to identify a third-order IFC, and if $\{\Phi_J\}$ is a minimal set of anharmonic force constants, enforcing the sum rules amounts to minimizing $\frac{1}{2}\sum_J \varphi_J^2$, where φ_J is the compensation to Φ_J, under a set of linear constraints

$$\sum_J A_{IJ}\left(\Phi_J + \varphi_J\right) = 0. \tag{28}$$

This can be solved by introducing a Lagrange multiplier λ_I for each of the constraints, leading to a new set of equations:

$$\sum_J \left[\sum_M A_{IM}A_{JM}\right]\lambda_J = -\sum_J A_{IJ}\Phi_J. \tag{29}$$

The values of the φ_J can be extracted from its solution as

$$\varphi_J = \sum_I \lambda_I A_{IJ}. \tag{30}$$

3. Examples

3.1. Si

The unquestionable position of Si as one of the most technologically important elements renders its thermal conductivity particularly crucial; moreover, the amount of accumulated knowledge about its manufacture enables the synthesis of high-quality samples for measurement. Thus, Si is one of the few materials for which the κ_ℓ of isotopically pure samples has been measured [49,50], which provides an ideal framework in which to test the implementation of anharmonic scattering in ShengBTE in isolation. A theoretical study using a similar methodology is also available [12] that achieves agreement with experiment within 5% at room temperature.

Bulk Si has a diamond structure. A possible parameterization of its irreducible unit cell has a projection of lattice vector α on Cartesian axis β equal to $0.5a_{\text{latt}}\left(1-\delta^{\alpha\beta}\right)$, where a_{latt} is the side length of the conventional cubic unit cell, and the two atoms of the motif placed at (0, 0, 0) and (1/4, 1/4, 1/4) in reduced coordinates.

To obtain the sets of IFCs for Si we followed the workflow presented in Fig. 1. For the DFT calculations we used `VASP` [32] with projector-augmented-wave (PAW) pseudopotentials [51], and Perdew–Burke–Ernzerhof (PBE) exchange and correlation functionals [52]. The plane-wave energy cutoff was chosen as 319 eV, equivalent to the maximum value recommended by the pseudopotential for Si plus an extra 30%. $11\times11\times11$ Monkhorst–Pack [53] **k**-point grids were used for structural minimization, while all supercell calculations used only the Γ point. We obtained a converged lattice parameter $a_{\text{latt}} = 5.47$ Å, in good agreement with experiment [54]. A $5\times5\times5$ supercell was employed for second-order calculations, but it was reduced to $4\times4\times4$ for the anharmonic ones. Only interactions up to fourth nearest neighbors were considered in the latter step, but no additional cutoff was imposed in the former.

Here we focus on the convergence of κ_ℓ with respect to BZ sampling density. Fig. 2 shows the values obtained for two different `scalebroad` settings: the default 1.0 and a less CPU-demanding 0.1 that can be expected to underestimate scattering to some degree. Each set of points is fitted to a curve of the form $\kappa_\ell = \kappa_\ell|_{N_1\to\infty}\left[1-e^{-N_1/A}\right]$ so that both its asymptotic value and its convergence rate can be estimated. Judging by the value of A, convergence with respect to $N_1 = N_2 = N_3$ is only weakly dependent on `scalebroad`: for instance, κ_ℓ reaches 90% of its converged value with a $15\times15\times15$ **q**-point grid in the `scalebroad` = 1.0 case, and with an $11\times11\times11$ grid when using `scalebroad` = 0.1. Moreover, the good agreement between the calculated points and the exponential curves suggests using this kind of fitting procedure as an acceleration method when dense BZ sampling would be prohibitively expensive.

In practice, achieving absolute convergence is seldom interesting, as variations in the thermal conductivity within at least a ∼5% interval can be expected even among experimental measurements on good quality samples [49]. Moreover, it is not unusual for the converged value of κ_ℓ to slightly overestimate the experimental results, since a variety of minor scattering sources (impurities,

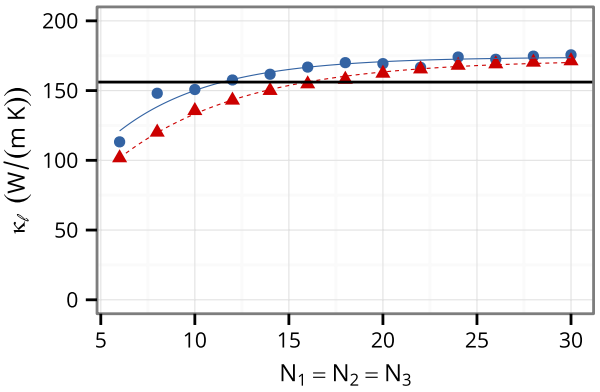

Fig. 2. Lattice thermal conductivity of isotopically pure ^{28}Si for different numbers of **q** points along each axis. Blue circles: results with `scalebroad` = 0.1; red triangles: results with `scalebroad` = 1.0. The solid blue and dashed red lines are fits of each set of points to a functional form $\kappa_\ell = \kappa_\ell|_{N_1\to\infty}\left[1 - e^{-N_1/A}\right]$. The experimental value [49] is shown as a thick horizontal black line.

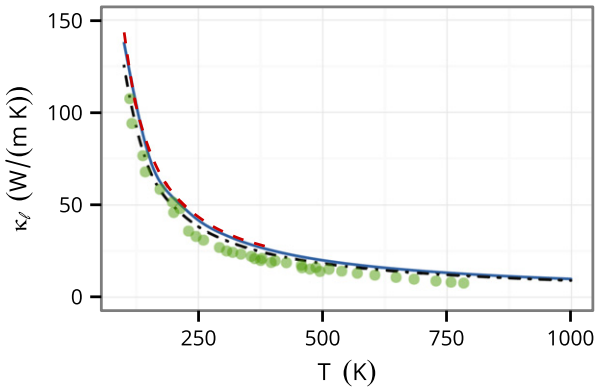

Fig. 3. Lattice thermal conductivity of natural InAs. Solid blue line: ShengBTE results with `scalebroad` = 0.1; dot–dash black line: refined ShengBTE calculation with `scalebroad` = 0.5; dashed red line: theoretical results from Ref. [23]; green circles: experimental data from Refs. [55–58].

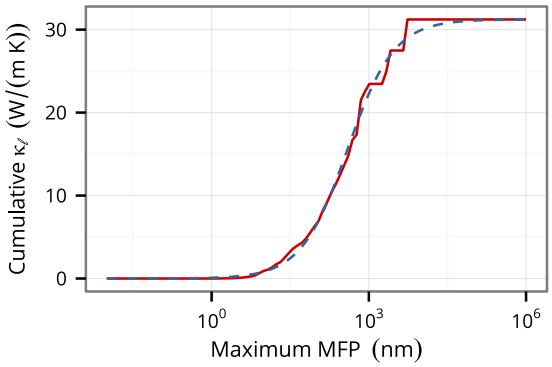

Fig. 4. Cumulative lattice thermal conductivity of InAs as a function of the maximum mean free path at 300 K. Solid red line: ShengBTE result. Dashed blue line: fit to a function of the form described by Eq. (31).

defects, residual isotopic disorder and so on) can be present in experimental samples. In addition to this, there are well known limitations to the accuracy with which DFT can predict quantities such as lattice constants and forces.

In this particular case, our extrapolation of κ_ℓ to $N_1 \to \infty$ yields a value of 172 W/(m K), around 10% higher than the experimental result for isotopically pure Si, 156 W/(m K). For comparison, the aforementioned independent theoretical result [12] obtains a value between 150 W/(m K) and 165 W/(m K).

As a final note regarding convergence, it is interesting to mention that for this system the iterative solution of the BTE converges in 5 steps and results in an increase in κ_ℓ of a mere ∼4% with respect to the relaxation-time approximation. This is consistent with the fact that phonon scattering is dominated by Umklapp processes; in such situations the RTA yields reasonable results. Only when normal processes are relevant can their treatment as resistive in the context of the RTA lead to significant errors.

3.2. InAs

Indium arsenide is a well known direct-bandgap III–V semiconductor with a zinc-blende structure. Its irreducible unit cell can be parameterized in a way analogous to that of Si except for the fact that each of the two atoms in the motif belongs to a different element. Experimental measurements of the thermal conductivity of InAs exist for different temperature ranges [55–58], as does an independent theoretical calculation using similar methods [23]. Therefore it is ideally well suited for validating our approach when isotope scattering and polar bonds are introduced into the picture.

The workflow we followed for obtaining sets of IFCs constants for InAs was very similar to the one presented in the previous subsection: the PBE approximation to exchange and correlation, PAW pseudopotentials, an energy cutoff of 311 eV – 30% above the maximum recommended cutoffs for In and As – and an 11 × 11 × 11 Monkhorst–Pack grid. We obtained a converged lattice parameter $a_{\text{latt}} = 6.06$ Å, again in very good agreement with the experiment [54]. We employed a 5 × 5 × 5 supercell for harmonic IFC calculation and a 4 × 4 × 4 one for the anharmonic IFCs. Additionally, we also used VASP to run a perturbative calculation of the dielectric parameters (dielectric tensor and Born effective charges).

We first performed a ShengBTE run with a 14 × 14 × 14 **q**-point grid (172 inequivalent **q** points) and `scalebroad` = 0.1. These parameters are very lax, and each temperature took only around 5 min running on a single processor on a desktop PC. The results are shown in Fig. 3 as a solid blue line and compared with the aforementioned independent studies [55–58,23]. Quite remarkably, even these rough values of κ_ℓ have predictive power; in fact, the performance of ShengBTE with these settings is comparable to the other set of theoretical results [23]. With this kind of configuration, our program can be a useful part of high-throughput studies, where sacrificing extreme accuracy for high performance is desirable [59]. The results can be improved by increasing `scalebroad` to 0.5, which yields the dot–dash curve in Fig. 3 at the price of increasing CPU time by a factor of 3. For temperatures $\lesssim$ 100 K this reciprocal-space sampling grid would probably be too coarse, since all significant contributions to the thermal conductivity come from a small volume around the Γ point. The theoretical overestimation of κ_ℓ with respect to experimental data in the high-temperature tail is a signature of the presence of n-phonon anharmonic processes [25,54] with $n > 3$.

Fig. 4 (solid red line) shows the room-temperature cumulative lattice thermal conductivity with respect to the maximum mean free path allowed, *i.e.*, the value of κ_ℓ when only phonons with a mean free path below a certain threshold are taken into account. The similarity of the curve to a logistic function when plotted with the horizontal axis in logarithmic scale suggests a fit to a uniparametric function of the form

$$\kappa_\ell\left(\Lambda \le \Lambda_{\max}\right) = \frac{\kappa_\ell}{1 + \frac{\Lambda_0}{\Lambda_{\max}}}. \tag{31}$$

This fit, included as a dashed blue curve in Fig. 4, reproduces both the slope and the position of the calculated data reasonably well. It yields a parameter $\Lambda_0 = 310$ nm that can be interpreted as representative of the mean free path of relevant heat-carrying

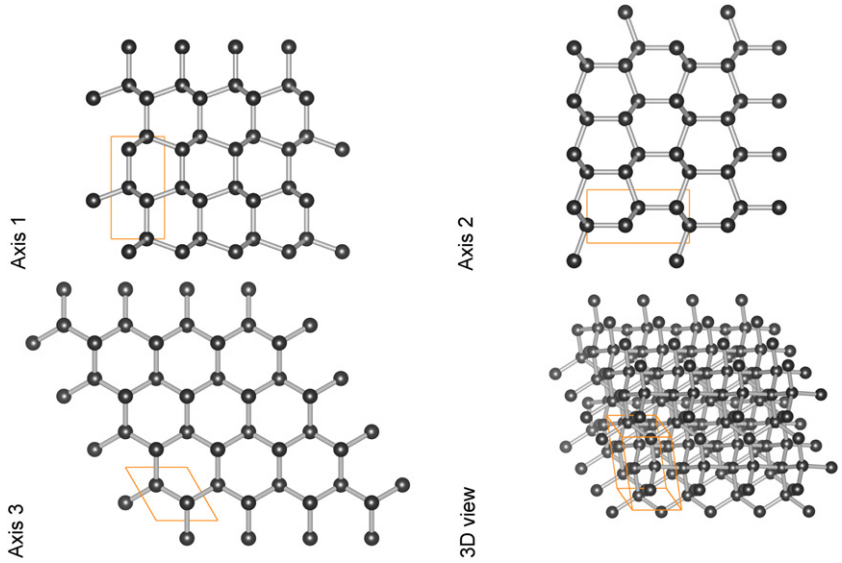

Fig. 5. Projections of the lonsdaleite crystal structure along the a, b, and c lattice vectors, and a 3D view of the whole structure. A particular unit cell is delimited by colored lines in all four panels.

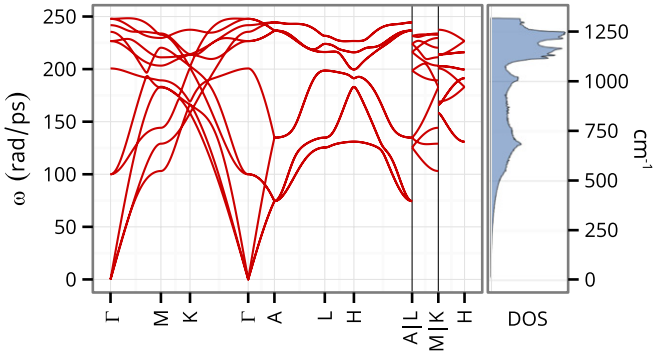

Fig. 6. Left: phonon spectrum of lonsdaleite along a path passing through the main high-symmetry points in the BZ [67]. Right: phonon density of states.

phonons in bulk InAs. This is important information when designing nanostructuring approaches to reducing κ_ℓ, for instance with thermoelectric applications in mind. A related quantity is the ratio $\kappa_\ell/\tilde{\kappa}_{SG}$, an estimate of the size at which nanostructuring dominates over anharmonic scattering; for InAs it is found to be 74 nm.

3.3. Lonsdaleite

Lonsdaleite (Fig. 5) is a hexagonal allotrope of carbon [60] structurally analogous to wurtzite. It is formed naturally from graphite in meteorites due to the huge stresses of impact, typically in association with ordinary diamond, and has also been synthesized by several methods [60–62]. Nevertheless, its physical properties have not been explored extensively: for instance, its electronic structure has only recently been calculated theoretically [63], and no report on its thermal conductivity exists so far.

Diamond has traditionally been placed at the top of the Mohs scale of mineral hardness. The reason behind this is the stiffness of sp^3 C–C bonds, which also leads to what is commonly considered the highest thermal conductivity among natural solids, around 2500 W/(m K) at room temperature [64]. Similarly graphite [64], consisting of parallel planes of carbon atoms with sp^2 hybridization, has a very high in-plane thermal conductivity (up to 1950 W/(m K) in high-grade samples); however, it is extremely anisotropic and the out-of-plane diagonal element of the conductivity tensor is around 300 times smaller [64]. A prediction for the thermal conductivity of lonsdaleite is thus extremely interesting due both to the lack of experimental data and to its relation to diamond and graphite. Intuitively, one would expect high values and an intermediate degree of anisotropy. It must be noted that lonsdaleite has been predicted to be significantly harder that diamond along certain crystallographic directions [65], which raises the question of whether it could also perform better as a thermal conductor.

From the point of view of sphere packing, lonsdaleite is hexagonal (*ABAB* . . . arrangement) whereas diamond is cubic (*ABCABC* . . . arrangement). Its hexagonal unit cell can be described in terms of two lengths, a and c, with cell vectors

$$\begin{aligned} \boldsymbol{\gamma}_1 &= a\left(\hat{\mathbf{x}}\cos\frac{\pi}{3} + \hat{\mathbf{y}}\sin\frac{\pi}{3}\right) \\ \boldsymbol{\gamma}_2 &= a\left(\hat{\mathbf{x}}\cos\frac{\pi}{3} - \hat{\mathbf{y}}\sin\frac{\pi}{3}\right) \\ \boldsymbol{\gamma}_3 &= \hat{\mathbf{z}}c. \end{aligned} \tag{32}$$

Experimental measurements of these two parameters [62] yield $a = 2.52$ Å and $c = 4.12$ Å, compatible with the ideal ratio $c/a = \sqrt{8/3}$ obtained in the sphere-packing picture. This parameterization of the lonsdaleite unit cell is completed by a tetra-atomic motif, with carbon atoms at (1/3, 2/3, 0), (2/3, 1/3, 1/2), (1/3, 2/3, 3/8) and (2/3, 1/3, 7/8).

In a VASP calculation employing parameters analogous to those in previous examples – and more specifically an energy cutoff of 520 eV – we obtain $a = 2.50$ Å and $c = 4.16$ Å, in fair agreement with experiment and affording a c/a ratio only slightly above the ideal value. The phonon spectrum of a $4 \times 4 \times 2$ supercell based on this equilibrium structure is shown in Fig. 6 along with the associated phonon density of states. As expected, both the acoustic and the optical branches have very high frequencies in comparison with other solids, with an upper bound comparable to the 250 rad/ps maximum frequency of diamond [66]. Group velocities of the acoustic modes near the Γ point are similarly high: 11.52, 11.99 and 18.56 km/s along the $\Gamma \to M$ line, and 11.34 and 19.56 km/s along $\Gamma \to A$. These numbers are a first indicator that the degree of anisotropy in this material is likely to be low.

Using the same supercell for anharmonic IFCs calculation, a $16 \times 16 \times 18$ **q**-point grid and a `scalebroad = 1.0` we obtain a converged thermal conductivity at 300 K of 1500 W/(m K) along the two degenerate directions and a slightly lower value,

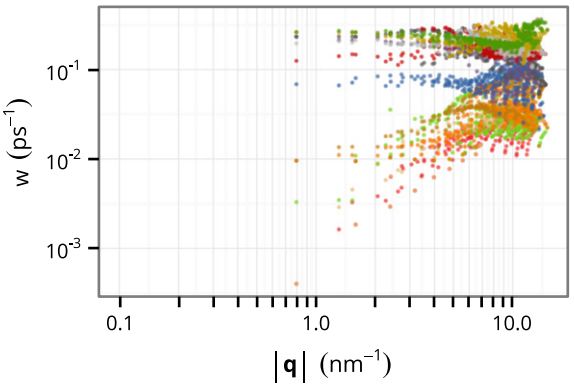

Fig. 7. Phonon scattering rates in lonsdaleite, computed on a $16 \times 16 \times 18$ **q**-point grid. Phonon branches are denoted by colors.

1270 W/(m K), along the *OZ* axis. For this material the RTA underestimates the diagonal elements of the thermal conductivity tensor by a very significant 20%. Thus, while lonsdaleite is still an exceptionally good thermal conductor when compared with metals and other solids, it seems to have the lowest conductivity among the three allotropes of carbon discussed in previous paragraphs. Moreover, in spite of the presence of an inequivalent axis in its structure, from the point of view of thermal conduction it has a low degree of anisotropy. As a final prediction, we also show in Fig. 7 the scattering rates of phonons in lonsdaleite as obtained from ShengBTE, which can eventually be checked against experimental line widths. It is worth noting that, even though κ_ℓ is quite robust to changes in **q**-sampling density and `scalebroad`, some of the individual scattering rates can be much more sensitive. Values of `scalebroad` close to 1.0 are recommended if accurate scattering rates are required. In the case of lonsdaleite, the larger number of atoms in the unit cell, the lower symmetry and the need to use `scalebroad` $= 1.0$ make the calculation much slower than those presented in the previous subsections for Si and InAs. The ShengBTE run took around one hour on 32 processors and required several GB of memory.

4. Conclusions

We have presented a program for the iterative solution of the linearized phonon Boltzmann equation in crystalline solids, including two- and three-phonon scattering processes computed from first principles. The program predicts materials' thermal conductivity tensors without any adjustable parameters. Among its most salient features are:

- a general implementation of point-group symmetries to optimize numerical integrals,
- an adaptive Gaussian broadening scheme so the method is completely parameter free, and
- its ability to deal with arbitrary three-dimensional lattices.

An original script for computing third-order IFCs for a general structure is also provided. This script employs a real-space, supercell-based approach, making full use of both point-group and translational symmetries to decrease the number of DFT calculations required.

Three example cases have been discussed, showing different features of the program in action. This range of examples covers isotropic as well as anisotropic systems, polar and nonpolar bonds and experimentally known as well as not-yet-measured conductivities. Experimental validation yields accuracy better than 10% in the available cases.

Our program enables the systematic computation and understanding of thermal conductivity in existing or hypothetical solid compounds. It can therefore be very valuable in the search of novel materials with targeted thermal conduction properties, and for the in-depth understanding of experimental measurements of thermal transport in solids.

Acknowledgments

The authors thank Prof. David Broido, Dr. Lucas Lindsay, Dr. Derek A. Stewart, Prof. Francesco Mauri and Dr. Nathalie Vast for insightful advice and independent results for validation of ShengBTE's output, Kinga Niedziółka and Prof. Philippe Jund for extensive beta testing, and Prof. Stefano Curtarolo for access to computational resources. This work was supported in part by ANR project ACCATTONE, EU project NEAT, and CEA project Carnot SIEVE.

Appendix. Input and output files

ShengBTE takes no command-line arguments and requires three input files to run: `CONTROL`, one of `FORCE_CONSTANTS_2ND` or `espresso.ifc2`, and `FORCE_CONSTANTS_3RD`. Full details about their formats can be found in the program's manual. `FORCE_CONSTANTS_2ND` can be generated directly by Phonopy and `FORCE_CONSTANTS_3RD` can be created with `thirdorder.py`. `CONTROL` contains all the parameters needed for the run apart from the force constants. It is written in the namelist format, which ensures a degree of flexibility and readability. The following is an example of a minimalistic `CONTROL` file that could be used to run a ShengBTE calculation for Si with a $17 \times 17 \times 17$ **q**-point grid and the default `scalebroad` $= 1.0$. It is assumed that the 2nd-order IFCs are in Phonopy format and that they come from a $5 \times 5 \times 5$ supercell. The cubic lattice parameter used is 5.47 Å.

```
&allocations
        nelements=1,
        natoms=2,
        ngrid(:)=17 17 17
&end
&crystal
        lfactor=0.547,
        lattvec(:,1)=0.0  0.5  0.5,
        lattvec(:,2)=0.5  0.0  0.5,
        lattvec(:,3)=0.5  0.5  0.0,
        elements="Si",
        types=1 1,
        positions(:,1)=0.00  0.00  0.00,
        positions(:,2)=0.25  0.25  0.25,
        scell(:)=5 5 5
&end
&parameters
        T=300.
&end
&flags
        nonanalytic=.FALSE.,
        nanowires=.FALSE.
&end
```

After running ShengBTE in the directory containing all three input files, the following outputs would be generated:

`BTE.qpoints`: list of irreducible q-points in the Brillouin zone obtained employed in the calculation.
`BTE.omega`: phonon angular frequencies at each of those q-points
`BTE.v`: group velocities of the phonon modes
`BTE.cv`: specific heat of the system per unit volume

`BTE.kappa_sg`: thermal conductivity per unit of mean free path in the small-grain limit
`BTE.dos`: phonon density of states
`BTE.pdos`: projected phonon density of states
`BTE.P3`: volume in phase space available for three-phonon processes
`BTE.P3_total`: sum of all the contributions in `BTE.P3`
`BTE.w_isotopic`: isotopic contribution to the scattering rate
`BTE.w_anharmonic`: contribution of three-phonon processes to the scattering rate
`BTE.w`: total zeroth-order scattering rates
`BTE.w_final`: total converged scattering rates
`BTE.kappa`: per-mode contributions to the thermal conductivity tensor
`BTE.kappa_tensor`: total thermal conductivity tensor
`BTE.kappa_scalar`: average of the diagonal elements of the thermal conductivity tensor
`BTE.cumulative_kappa_*`: this set of files is analogous to `BTE.kappa*`, except in that their first column specifies a cutoff mean free path for phonons

Users are strongly encouraged to read the manual, which contains additional information about these files.

References

[1] M. Zebarjadi, K. Esfarjani, M.S. Dresselhaus, Z.F. Ren, G. Chen, Perspectives on thermoelectrics: from fundamentals to device applications, Energy Environ. Sci. 5 (2012) 5147–5162.
[2] L.-T. Yeh, R.C. Chu, Thermal Management of Microloectronic Equipment: Heat Transfer Theory, Analysis Methods, and Design Practices, ASME Press, 2002.
[3] C.D. Wright, L. Wang, P. Shah, M. Aziz, E. Varesi, R. Bez, M. Moroni, F. Cazzaniga, The design of rewritable ultrahigh density scanning-probe phase-change memories, IEEE Trans. Nanotechnol. 10 (2011) 900–912.
[4] G.M. Manthilake, N.d. Koker, D.J. Frost, C.A. McCammon, Lattice thermal conductivity of lower mantle minerals and heat flux from Earth's core, Proc. Natl. Acad. Sci. USA 108 (2011) 17901–17904.
[5] J.M. Ziman, Electrons and Phonons: The Theory of Transport Phenomena in Solids, Clarendon Press, 1960.
[6] J. Callaway, Model for lattice thermal conductivity at low temperatures, Phys. Rev. 113 (1959) 1046–1051.
[7] P.B. Allen, Improved callaway model for lattice thermal conductivity, Phys. Rev. B 88 (2013) 144302.
[8] M. Omini, A. Sparavigna, An iterative approach to the phonon Boltzmann equation in the theory of thermal conductivity, Physica B 212 (1995) 101–112.
[9] M. Omini, A. Sparavigna, Beyond the isotropic-model approximation in the theory of thermal conductivity, Phys. Rev. B 53 (1996) 9064.
[10] M. Omini, A. Sparavigna, Heat transport in dielectric solids with diamond structure, Nuovo Cimento D 19 (1997) 1537.
[11] G. Deinzer, G. Birner, D. Strauch, *Ab initio* calculation of the linewidth of various phonon modes in germanium and silicon, Phys. Rev. B 67 (2003) 144304.
[12] D.A. Broido, M. Malorny, G. Birner, N. Mingo, D.A. Stewart, Intrinsic lattice thermal conductivity of semiconductors from first principles, Appl. Phys. Lett. 91 (2007) 231922.
[13] K. Esfarjani, H.T. Stokes, Method to extract anharmonic force constants from first principles calculations, Phys. Rev. B 77 (2008) 144112.
[14] X. Tang, J. Dong, Pressure dependence of harmonic and anharmonic lattice dynamics in MgO: a first-principles calculation and implications for lattice thermal conductivity, Phys. Earth Planet. Inter. 174 (2009) 33–38.
[15] X. Tang, J. Dong, Lattice thermal conductivity of MgO at conditions of earth's interior, Proc. Natl. Acad. Sci. USA 107 (2010) 4539–4543.
[16] A. Ward, D.A. Broido, Intrinsic phonon relaxation times from first-principles studies of the thermal conductivities of Si and Ge, Phys. Rev. B 81 (2010) 085205.
[17] A. Ward, D.A. Broido, D.A. Stewart, G. Deinzer, Ab initio theory of the lattice thermal conductivity in diamond, Phys. Rev. B 80 (2009) 125203.
[18] G. Fugallo, M. Lazzeri, L. Paulatto, F. Mauri, *Ab initio* variational approach for evaluating lattice thermal conductivity, Phys. Rev. B 88 (2013) 045430.
[19] J. Garg, N. Bonini, B. Kozinsky, N. Marzari, Role of disorder and anharmonicity in the thermal conductivity of silicon–germanium alloys: a first-principles study, Phys. Rev. Lett. 106 (2011) 045901.
[20] Z. Tian, J. Garg, K. Esfarjani, T. Shiga, J. Shiomi, G. Chen, Phonon conduction in PbSe, PbTe, and $PbTe_{1-x}Se_x$ from first-principles calculations, Phys. Rev. B 85 (2012) 184303.
[21] L. Lindsay, D.A. Broido, T.L. Reinecke, Thermal conductivity and large isotope effect in GaN from first principles, Phys. Rev. Lett. 109 (2012) 095901.
[22] W. Li, L. Lindsay, D.A. Broido, D.A. Stewart, N. Mingo, Thermal conductivity of bulk and nanowire $Mg_2Si_xSn_{1-x}$ alloys from first principles, Phys. Rev. B 86 (2012) 174307.
[23] L. Lindsay, D.A. Broido, T.L. Reinecke, Ab initio thermal transport in compound semiconductors, Phys. Rev. B 87 (2013) 165201.
[24] H. Dekura, T. Tsuchiya, J. Tsuchiya, *Ab initio* lattice thermal conductivity of $MgSiO_3$ perovskite as found in earth's lower mantle, Phys. Rev. Lett. 110 (2013) 025904.
[25] W. Li, N. Mingo, Thermal conductivity of bulk and nanowire InAs, AlN, and BeO polymorphs from first principles, J. Appl. Phys. 114 (2013) 183505.
[26] J.W.L. Pang, W.J.L. Buyers, A. Chernatynskiy, M.D. Lumsden, B.C. Larson, S.R. Phillpot, Phonon lifetime investigation of anharmonicity and thermal conductivity of UO_2 by neutron scattering and theory, Phys. Rev. Lett. 110 (2013) 157401.
[27] L. Lindsay, D.A. Broido, T.L. Reinecke, First-principles determination of ultrahigh thermal conductivity of boron arsenide: a competitor for diamond? Phys. Rev. Lett. 111 (2013) 025901.
[28] N. Bonini, J. Garg, N. Marzari, Acoustic phonon lifetimes and thermal transport in free-standing and strained graphene, Nano Lett. 12 (2012) 2673–2678.
[29] W. Li, J. Carrete, N. Mingo, Thermal conductivity and phonon linewidths of monolayer MoS_2 from first principles, Appl. Phys. lett. 103 (2013) 253103.
[30] W. Li, N. Mingo, L. Lindsay, D.A. Broido, D.A. Stewart, N.A. Katcho, Thermal conductivity of diamond nanowires from first principles, Phys. Rev. B 85 (2012) 195436.
[31] N. Mingo, D. Stewart, D. Broido, L. Lindsay, W. Li, *Ab initio* thermal transport, in: Length-Scale Dependent Phonon Interactions, Springer, 2014, pp. 137–173.
[32] G. Kresse, J. Furthmüller, Efficient iterative schemes for *ab initio* total-energy calculations using a plane-wave basis set, Phys. Rev. B 54 (1996) 11169–11186.
[33] P. Giannozzi, S. Baroni, N. Bonini, M. Calandra, R. Car, C. Cavazzoni, D. Ceresoli, G.L. Chiarotti, M. Cococcioni, I. Dabo, A. Dal Corso, S. de Gironcoli, S. Fabris, G. Fratesi, R. Gebauer, U. Gerstmann, C. Gougoussis, A. Kokalj, M. Lazzeri, L. Martin-Samos, N. Marzari, F. Mauri, R. Mazzarello, S. Paolini, A. Pasquarello, L. Paulatto, C. Sbraccia, S. Scandolo, G. Sclauzero, A.P. Seitsonen, A. Smogunov, P. Umari, R.M. Wentzcovitch, QUANTUM ESPRESSO: a modular and open-source software project for quantum simulations of materials, J. Phys.: Condens. Matter 21 (2009) 395502.
[34] A. Togo, F. Oba, I. Tanaka, First-principles calculations of the ferroelastic transition between rutile-type and $CaCl_2$-type SiO_2 at high pressures, Phys. Rev. B 78 (2008) 134106.
[35] N.A. Spaldin, A beginner's guide to the modern theory of polarization, J. Solid State Chem. 195 (2012) 2–10.
[36] R.M. Pick, M.H. Cohen, R.M. Martin, Microscopic theory of force constants in the adiabatic approximation, Phys. Rev. B 1 (1970) 910–920.
[37] X. Gonze, J.-C. Charlier, D.C. Allan, M.P. Teter, Interatomic force constants from first principles: the case of α-quartz, Phys. Rev. B 50 (1994) 13035–13038.
[38] Y. Wang, J.J. Wang, W.Y. Wang, Z.G. Mei, S.L. Shang, L.Q. Chen, Z.K. Liu, A mixed-space approach to first-principles calculations of phonon frequencies for polar materials, J. Phys.: Condens. Matter 22 (2010) 202201.
[39] R.E. Peierls, Zur kinetischen theorie der warmeleitung in kristallen, Ann. Phys. Lpz. 3 (1929) 1055–1101.
[40] L. Lindsay, D.A. Broido, Three-phonon phase space and lattice thermal conductivity in semiconductors, J. Phys.: Condens. Matter 20 (2008) 165209.
[41] A. Kundu, N. Mingo, D.A. Broido, D.A. Stewart, Role of light and heavy embedded nanoparticles on the thermal conductivity of SiGe alloys, Phys. Rev. B 84 (2011) 125426.
[42] S.-I. Tamura, Isotope scattering of dispersive phonons in Ge, Phys. Rev. B 27 (1983) 858–866.
[43] M. Berglund, M.E. Wieser, Isotopic compositions of the elements 2009 (IUPAC technical report), Pure Appl. Chem. 83 (2011) 397–410.
[44] A. Togo, `spglib`, a C library for finding and handling crystal symmetries, http://spglib.sourceforge.net/.
[45] R.G. Chambers, The conductivity of thin wires in a magnetic field, Proc. R. Soc. Lond. Ser. A 202 (1950) 378.
[46] F. Favot, A.D. Corso, Phonon dispersions: performance of the generalized gradient approximation, Phys. Rev. B 60 (1999) 11427.
[47] A.D. Corso, Ab initio phonon dispersions of transition and noble metals: effects of the exchange and correlation functional, J. Phys.: Condens. Matter 25 (2013) 145401.
[48] D.A. Broido, L. Lindsay, T.L. Reinecke, Ab initio study of the unusual thermal transport properties of boron arsenide and related materials, Phys. Rev. B 88 (2013) 214303.
[49] R.K. Kremer, K. Graf, M. Cardona, G.G. Devyatykh, A.V. Gusev, A.M. Gibin, A.V. Inyushkin, A.N. Taldenkov, H.-J. Pohl, Thermal conductivity of isotopically enriched 28Si: revisited, Solid State Commun. 131 (2004) 499–503.
[50] A.V. Inyushkin, A.N. Taldenkov, A.M. Gibin, A.V. Gusev, H.-J. Pohl, On the isotope effect in thermal conductivity of silicon, Phys. Status Solidi C 1 (2004) 2995–2998.
[51] P.E. Blöchl, Projector augmented-wave method, Phys. Rev. B 50 (1994) 17953–17979.
[52] J.P. Perdew, K. Burke, M. Ernzerhof, Generalized gradient approximation made simple, Phys. Rev. Lett. 77 (1996) 3865–3868.
[53] H.J. Monkhorst, J.D. Pack, Special points for Brillouin-zone integrations, Phys. Rev. B 13 (1976) 5188–5192.
[54] M.M.E. Levinshtein, S.L. Rumyantsev, M. Shur, Handbook Series on Semiconductor Parameters. 1. Si, Ge, C (diamond), GaAs, GaP, GaSb, InAs, InP, InSb, World Scientific Publishing, 1996.
[55] P.V. Tamarin, S.S. Shalyt, Thermal conductivity and thermoelectric power of indium arsenide at low temperatures, Sov. Phys. Semicond. 5 (1971) 1097–1098.

[56] G. LeGuillou, H.J. Albany, Phonon conductivity of InAs, Phys. Rev. B 5 (1972) 2301–2308.
[57] A.S. Okhotin, A.S. Pushkarskii, V.V. Gorbachev, Thermophysical Properties of Semiconductors, Atom Publ. House, 1972.
[58] R. Bowers, R.W. Ure Jr, J.E. Bauerle, A.J. Cornish, InAs and InSb as thermoelectric materials, J. Appl. Phys. 30 (2004) 930–934.
[59] S. Curtarolo, G.L.W. Hart, M. Buongiorno Nardelli, N. Mingo, S. Sanvito, O. Levy, The high-throughput highway to computational materials design, Nature Mater. 12 (2013) 191–201.
[60] C. Frondel, U.B. Marvin, Lonsdaleite, a hexagonal polymorph of diamond, Nature 214 (1967) 587–589.
[61] S. Bhargava, H.D. Bist, S. Sahli, M. Aslam, H.B. Tripathi, Diamond polytypes in the chemical vapor deposited diamond films, Appl. Phys. Lett. 67 (1995) 1706.
[62] F.P. Bundy, J.S. Kasper, Hexagonal diamond—a new form of carbon, J. Chem. Phys. 46 (2004) 3437.
[63] A. De, C.E. Pryor, Electronic structure and optical properties of the lonsdaleite phase of Si, Ge and diamond, arXiv e-print 1210.7392, 2012. http://arxiv.org/abs/1210.7392.
[64] M. Inagaki, F. Kang, M. Toyoda, H. Konno, Advanced Materials Science and Engineering of Carbon, Butterworth-Heinemann, 2013.
[65] Z. Pan, H. Sun, Y. Zhang, C. Chen, Harder than diamond: superior indentation strength of wurtzite BN and lonsdaleite, Phys. Rev. Lett. 102 (2009) 055503.
[66] J.L. Warren, J.L. Yarnell, G. Dolling, R.A. Cowley, Lattice dynamics of diamond, Phys. Rev. 158 (1967) 805–808.
[67] W. Setyawan, S. Curtarolo, High-throughput electronic band structure calculations: challenges and tools, Comput. Math. Sci. 49 (2010) 299–312.